

Dynamic crack analysis of fiber reinforced piezoelectric composites by a Galerkin BEM

†*M. Wünsche¹, J. Sladek¹, V. Sladek¹ and Ch. Zhang²

¹Institute of Construction and Architecture, Slovak Academy of Sciences, 84503 Bratislava, Slovakia

²School of Science and Technology, Chair of Structural Mechanics, University of Siegen, D-57068 Siegen, Germany

*Presenting author: wuensche@bauwesen.uni-siegen.de

†Corresponding author: wuensche@bauwesen.uni-siegen.de

Abstract

In this paper, transient dynamic analysis of micro-cracks of arbitrary shape in two-dimensional, linear piezoelectric fiber reinforced composite materials is presented. Interface cracks between fiber and matrix as well as cracks inside the matrix and fibers are analyzed. A symmetric Galerkin time-domain boundary element method in conjunction with a multi-domain technique is developed for this purpose. The time discretization is performed by a collocation method and time-domain fundamental solutions for piezoelectric materials are applied. An explicit time-stepping scheme is obtained to compute the discrete boundary data including the generalized crack-opening-displacements (CODs). Iterative solution algorithms are implemented to treat the non-linear semi-permeable electrical crack-face boundary conditions and for a crack-face contact analysis at time-steps when a physically unacceptable crack-face intersection occurs. Numerical examples are presented to reveal the effects of the micro-cracks, the material combinations and the dynamic loading on the intensity factors and the scattered wave fields.

Keywords: piezoelectric fiber composites, interface cracks, impact loading, complex intensity factors, time-domain BEM.

Introduction

Piezoelectric materials are widely applied in smart structures like transducers, actuators and sensors by utilizing the property of converting electrical energy into mechanical energy and vice versa. In recent years piezoelectric fiber reinforced materials have received increasing attention. A special class of such composites combines piezoelectric ceramics or polymers as active fibers with passive non-piezoelectric materials as matrix. Fiber reinforced materials can be optimized to satisfy the high performance requirements by taking advantages of the most beneficial properties of each constituent. Piezoelectric ceramics are very brittle with low fracture toughness and micro as well as macro cracks may be induced during the manufacturing and under the in-service condition. Beside cracks inside the homogeneous matrix and fibers, interface cracks play an important role for the design and safety of real structures. Since the electrical permittivity of the crack medium has a significant influence on the intensity factors the crack-face boundary conditions have to be described properly. Although the analysis of cracks in homogenous piezoelectric solids under static and dynamic loadings has been presented by many authors the corresponding analysis of interface cracks in piezoelectric fiber reinforced materials is rather limited due to the problem complexity. This paper presents such an analysis by using a hypersingular symmetric Galerkin boundary element method (SGBEM) for crack problems in two-dimensional (2D), fiber reinforced and linear piezoelectric solids.

Problem statement and numerical solution algorithm

We consider a piecewise homogeneous linear piezoelectric fiber-matrix structure with cracks of arbitrary shape. In the absence of body forces, free electric charges and using quasi-electrostatic

assumption, the cracked solid satisfies the generalized constitutive equations

$$\sigma_{iJ}(\mathbf{x}, t) = C_{iJKl}^\lambda u_{K,l}(\mathbf{x}, t) \quad (1)$$

and the generalized equations of motion

$$\sigma_{iJ,i}(\mathbf{x}, t) = \rho^\lambda \delta_{JK}^* \ddot{u}_K(\mathbf{x}, t), \quad \delta_{JK}^* = \begin{cases} \delta_{jk}, & J = j; K = k, \\ 0, & \text{otherwise,} \end{cases} \quad (2)$$

the initial conditions

$$u_I(\mathbf{x}, t = 0) = \dot{u}_I(\mathbf{x}, t = 0) = 0, \quad (3)$$

the boundary conditions

$$u_I(\mathbf{x}, t) = \bar{u}_I(\mathbf{x}, t), \quad \mathbf{x} \in \Gamma_u, \quad (4)$$

$$t_I(\mathbf{x}, t) = \bar{t}_I(\mathbf{x}, t), \quad \mathbf{x} \in \Gamma_t, \quad (5)$$

and the continuity as well as the equilibrium conditions on the interface between the fiber and the matrix except the crack-faces

$$u_I^I(\mathbf{x}, t) = u_I^{II}(\mathbf{x}, t), \quad \mathbf{x} \in \Gamma_{if}, \quad (6)$$

$$t_I^I(\mathbf{x}, t) = -t_I^{II}(\mathbf{x}, t), \quad \mathbf{x} \in \Gamma_{if}, \quad (7)$$

with the lower case letter subscripts $j \in \{1, 2\}$ and the capital letter subscripts $J \in \{1, 2, 4\}$, respectively. The generalized displacements u_I , the generalized tractions t_I , the generalized stresses σ_{iJ} and the generalized elasticity tensor C_{iJKl}^λ for a homogenous domain Ω^λ ($\lambda = 1, 2, \dots, N$) are defined by

$$u_I = \begin{cases} u_i, & I = i & \text{(mechanical displacements)} \\ \varphi, & I = 4 & \text{(electrical potential)} \end{cases}, \quad (8)$$

$$\sigma_{iJ} = \begin{cases} \sigma_{ij}, & J = j & \text{(mechanical stresses)} \\ D_i, & J = 4 & \text{(electrical displacements)} \end{cases}, \quad (9)$$

$$C_{iJKl} = \begin{cases} c_{ijkl}, & J = j; K = k & \text{(elasticity tensor)} \\ e_{lij}, & J = j; K = 4 & \text{(piezoelectric tensor)} \\ e_{ikl}, & J = 4; K = k & \text{(piezoelectric tensor)} \\ -\kappa_{il}, & J = K = 4 & \text{(electrical permittivity tensor)} \end{cases}, \quad (10)$$

$$t_I(\mathbf{x}, t) = \sigma_{jI}(\mathbf{x}, t) e_j(\mathbf{x}). \quad (11)$$

In the Eqs. (1)-(11), e_j , u_i , σ_{ij} , φ and D_i are the outward unit normal vector, the mechanical displacements, the stresses, the electrical potential and the electrical displacements. Further, ρ , C_{ijkl} , e_{ijk} and κ_{ij} represent the mass density, the elasticity tensor, the piezoelectric tensor and the dielectric permittivity tensor. Γ_t and Γ_u define the external boundaries where the tractions t_I and the displacements u_I are prescribed, while Γ_{if} is the interface between the homogenous domains Ω^λ ($\lambda = 1, 2, \dots, N$).

On the crack-faces three different electrical boundary conditions are considered. As an extension of the mostly applied traction-free crack-face boundary condition in linear elastic fracture mechanics it has been suggested in [4] to consider the crack as impermeable for the electrical field

$$D_2(\mathbf{x} \in \Gamma_{c^+}, t) = D_2(\mathbf{x} \in \Gamma_{c^-}, t) = 0. \quad (12)$$

$\Gamma_{c\pm}$ denotes the upper and the lower crack-faces. Another in [5] introduced model treats the crack as fully electrical permeable

$$D_2(\mathbf{x} \in \Gamma_{c+}, t) = D_2(\mathbf{x} \in \Gamma_{c-}, t), \quad \varphi(\mathbf{x} \in \Gamma_{c+}, t) - \varphi(\mathbf{x} \in \Gamma_{c-}, t) = 0. \quad (13)$$

This implies identical potentials on both crack-faces or in other words the crack exists only for the mechanical and not for the electrical field. In both models, the limited dielectric properties of the interior of the crack are not taken into account. Due to this fact a more realistic semi-permeable crack-face boundary condition has been introduced as [2]

$$D_2(\mathbf{x} \in \Gamma_{c+}, t) = D_2(\mathbf{x} \in \Gamma_{c-}, t) = -\kappa_c \frac{\varphi(\mathbf{x} \in \Gamma_{c+}, t) - \varphi(\mathbf{x} \in \Gamma_{c-}, t)}{u_2(\mathbf{x} \in \Gamma_{c+}, t) - u_2(\mathbf{x} \in \Gamma_{c-}, t)}, \quad (14)$$

where $\kappa_c = \kappa_r \kappa_0$ is the product of the relative permittivity of the considered crack medium κ_r and the permittivity of the vacuum $\kappa_0 = 8.854 \cdot 10^{-12} C/(Vm)$. D_2 and u_2 are the normal components of the electrical displacements and the mechanical displacements on the crack-faces. This crack-face boundary condition has been further improved by including electrostatic tractions [3], [1]. The generalized crack-opening-displacements (CODs) are defined by

$$\Delta u_I(\mathbf{x}, t) = u_I(\mathbf{x} \in \Gamma_{c+}, t) - u_I(\mathbf{x} \in \Gamma_{c-}, t). \quad (15)$$

Throughout the paper, a comma after a quantity represents spatial derivatives while a dot over the quantity denotes time differentiation. Lower case Latin indices take the values 1 and 2 (elastic), while capital Latin indices take the values 1, 2 (elastic) and 4 (electric). Unless otherwise stated, the conventional summation rule over repeated indices is implied.

Time-domain boundary integral equations and fundamental solutions

A spatial Galerkin-method is implemented to solve the initial-boundary value problem with the boundary element method. This demands that the time-domain boundary integral equations (BIEs) are treated in a weighted residual sense. The generalized time-domain displacement and traction BIEs can be written as [8]

$$\begin{aligned} & \int_{\Gamma} \psi(\mathbf{x}) u_J(\mathbf{x}, t) d\Gamma_x = \\ & \int_{\Gamma} \psi(\mathbf{x}) \int_{\Gamma_b} \left[u_{IJ}^G(\mathbf{x}, \mathbf{y}, t) * t_I(\mathbf{y}, t) - t_{IJ}^G(\mathbf{x}, \mathbf{y}, t) * u_I(\mathbf{y}, t) \right] d\Gamma_y d\Gamma_x \\ & + \int_{\Gamma} \psi(\mathbf{x}) \int_{\Gamma_{c+}} t_{IJ}^G(\mathbf{x}, \mathbf{y}, t) * \Delta u_I(\mathbf{y}, t) d\Gamma_y d\Gamma_x, \end{aligned} \quad (16)$$

$$\begin{aligned} & \int_{\Gamma} \psi(\mathbf{x}) t_J(\mathbf{x}, t) d\Gamma_x = \\ & \int_{\Gamma} \psi(\mathbf{x}) \int_{\Gamma_b} \left[v_{IJ}^G(\mathbf{x}, \mathbf{y}, t) * t_I(\mathbf{y}, t) - w_{IJ}^G(\mathbf{x}, \mathbf{y}, t) * u_I(\mathbf{y}, t) \right] d\Gamma_y d\Gamma_x \\ & + \int_{\Gamma} \psi(\mathbf{x}) \int_{\Gamma_{c+}} w_{IJ}^G(\mathbf{x}, \mathbf{y}, t) * \Delta u_I(\mathbf{y}, t) d\Gamma_y d\Gamma_x, \end{aligned} \quad (17)$$

where $\psi(x)$ is the weight or test function, $\Gamma_b = \Gamma_u + \Gamma_t + \Gamma_{if}$, an asterisk denotes the Riemann convolution

$$g(\mathbf{x}, t) * h(\mathbf{x}, t) = \int_0^t g(\mathbf{x}, t - \tau)h(\mathbf{x}, \tau)d\tau \quad (18)$$

and the dynamic displacement, traction and higher-order traction fundamental solutions are defined by

$$t_{IJ}^G(\mathbf{x}, \mathbf{y}, t) = C_{qIKr}e_q(\mathbf{y})u_{KJ,r}^G(\mathbf{x}, \mathbf{y}, t), \quad (19)$$

$$v_{IJ}^G(\mathbf{x}, \mathbf{y}, t) = -C_{pIKs}e_p(\mathbf{x})u_{KJ,s}^G(\mathbf{x}, \mathbf{y}, t), \quad (20)$$

$$w_{IJ}^G(\mathbf{x}, \mathbf{y}, t) = C_{pIKs}e_p(\mathbf{x})C_{qJLr}e_q(\mathbf{y})u_{KL,sr}^G(\mathbf{x}, \mathbf{y}, t). \quad (21)$$

The fundamental solutions possess the following spatial symmetry properties

$$u_{IJ}^G(\mathbf{x}, \mathbf{y}, t) = u_{JI}^G(\mathbf{y}, \mathbf{x}, t), \quad (22)$$

$$t_{IJ}^G(\mathbf{x}, \mathbf{y}, t) = -v_{IJ}^G(\mathbf{x}, \mathbf{y}, t) = v_{JI}^G(\mathbf{y}, \mathbf{x}, t), \quad (23)$$

$$w_{IJ}^G(\mathbf{x}, \mathbf{y}, t) = w_{JI}^G(\mathbf{y}, \mathbf{x}, t). \quad (24)$$

These symmetry properties (22)-(24) can be used to derive a spatial symmetric Galerkin-method. This is achieved if the displacement Galerkin-BIEs (16) are applied on the external boundary Γ_u where the generalized displacements are known and the interface Γ_{if} for the generalized tractions, while the traction Galerkin-BIEs (17) are used on the external boundary Γ_t where the generalized tractions are prescribed and the interface Γ_{if} for the generalized displacements.

The time-domain fundamental solutions for homogeneous linear piezoelectric solids [7] are implemented in this work. They are expressed in the 2D case by a line integral over a unit circle as

$$u_{IJ}^G(\mathbf{x}, \mathbf{y}, t) = \frac{H(t)}{4\pi^2} \int_{|\mathbf{n}|=1} \sum_{m=1}^3 \frac{P_{IJ}^m}{\rho c_m} \frac{1}{c_m t + \mathbf{n} \cdot (\mathbf{y} - \mathbf{x})} d\mathbf{n}, \quad (25)$$

where $H(t)$, \mathbf{n} , c_m and P_{IJ}^m denote the Heaviside step function, the wave propagation vector, the phase velocities of the elastic waves and the projector. By integration by parts and applying the properties of the time convolution the time-domain generalized displacement fundamental solutions can be divided into a singular static and a regular dynamic part as

$$u_{IJ}^G(\mathbf{x}, \mathbf{y}, t) * f(t) = u_{IJ}^S(\mathbf{x}, \mathbf{y})f(t) + u_{IJ}^D(\mathbf{x}, \mathbf{y}, t) * \dot{f}(t). \quad (26)$$

In the same way, the traction and the higher-order traction fundamental solutions can also be divided into their singular static and regular dynamic parts [8].

Numerical solution algorithm

To solve the time-domain BIEs (16) and (17) a numerical solution procedure is presented in the following. The Galerkin-method is used for the spatial discretization while a collocation method is utilized for the temporal discretization [9]. The piezoelectric solid is divided into several sub-domains with homogeneous material properties and to each sub-domain the time-domain BIEs (16) and (17) are applied. For the spatial discretization, the crack-faces, the external boundary of each homogeneous sub-domain and the interfaces of the cracked solid are discretized by linear elements. Linear shape functions are also used for the temporal discretization in the present analysis. At the crack-tips inside a homogeneous sub-domain, special crack-tip elements are applied to describe the local behaviour of the generalized CODs near the crack-tips

properly. This ensures an accurate and a direct calculation of the intensity factors from the numerically computed CODs. On the other hand, the asymptotic crack-tip field in the case of an interfacial crack between two dissimilar piezoelectric materials shows different oscillating and non-oscillating singularities in the generalized stress field [6], which makes an implementation of special crack-tip elements quite cumbersome. For this reason, only standard elements are applied at the crack-tips for interface cracks. The strongly singular and hypersingular boundary integrals can be computed analytically. By using linear temporal shape-functions, time integrations can also be performed analytically. Only the line integrals over the unit circle arising in the regular parts of the dynamic fundamental solutions have to be computed numerically by the standard Gaussian quadrature.

After temporal and spatial discretizations and considering the initial conditions the following systems of linear algebraic equations can be obtained for each sub-domain Ω^ζ ($\zeta = 1, 2, \dots, N$)

$$\begin{aligned} \mathbf{C}_\zeta \mathbf{u}_\zeta^K = & \mathbf{U}_\zeta^S \mathbf{t}_\zeta^K - \mathbf{T}_\zeta^S \mathbf{u}_\zeta^K + \mathbf{T}_\zeta^S \Delta \mathbf{u}_\zeta^K \\ & + \sum_{k=1}^K \left[\mathbf{U}_\zeta^{D;K-k+1} \mathbf{t}_\zeta^k - \mathbf{T}_\zeta^{D;K-k+1} \mathbf{u}_\zeta^k + \mathbf{T}_\zeta^{D;K-k+1} \Delta \mathbf{u}_\zeta^k \right], \end{aligned} \quad (27)$$

$$\begin{aligned} \mathbf{D}_\zeta \mathbf{t}_\zeta^K = & \mathbf{V}_\zeta^S \mathbf{t}_\zeta^K - \mathbf{W}_\zeta^S \mathbf{u}_\zeta^K + \mathbf{W}_\zeta^S \Delta \mathbf{u}_\zeta^K \\ & + \sum_{k=1}^K \left[\mathbf{V}_\zeta^{D;K-k+1} \mathbf{t}_\zeta^k - \mathbf{W}_\zeta^{D;K-k+1} \mathbf{u}_\zeta^k + \mathbf{W}_\zeta^{D;K-k+1} \Delta \mathbf{u}_\zeta^k \right]. \end{aligned} \quad (28)$$

By invoking the continuity conditions (6) and (7) on the interface Γ_{if} as well as (12), (13) or (14) on the crack-faces Γ_{c+} and Γ_{c-} and by considering the boundary conditions (4) and (5), the following explicit time-stepping scheme can be obtained

$$\mathbf{x}^K = (\Xi^1)^{-1} \left[\Upsilon^1 \mathbf{y}^K + \sum_{k=1}^{K-1} \left(\Lambda^{K-k+1} \mathbf{t}^k - \Theta^{K-k+1} \mathbf{u}^k \right) \right], \quad (29)$$

where Ξ^1 and Υ^1 are the system matrices, \mathbf{y}^K is the vector of the prescribed boundary data while \mathbf{x}^K represents the vector of the unknown boundary data, which can be computed time-step by time-step.

The dynamic intensity factors for a crack-tip inside a homogeneous domain or on the interface are defined in [6] and [8]. They are obtained directly from the numerically computed generalized CODs.

Numerical examples

In the following, numerical examples are presented and discussed. To measure the intensity of the electrical loading the parameter

$$\chi = \frac{e_{22} D_0}{\kappa_{22} \sigma_0} \quad (30)$$

is introduced, with σ_0 and D_0 being the mechanical and electrical loading amplitudes. For convenience, the mode-I, the mode-II and the mode-IV dynamic intensity factors for crack-tips inside a homogeneous sub-domain are normalized by

$$K_I^*(t) = \frac{K_I(t)}{K_0}, \quad K_{II}^*(t) = \frac{K_{II}(t)}{K_0}, \quad K_{IV}^*(t) = \frac{e_{22} K_{IV}(t)}{\varepsilon_{22} K_0}. \quad (31)$$

In the same way, the real part K_1 and the imaginary part K_2 of the complex dynamic stress intensity factor and the electrical displacement intensity factor K_4 for interface cracks are normalized by

$$K_1^*(t) = \frac{K_1(t)}{K_0}, \quad K_2^*(t) = \frac{K_2(t)}{K_0}, \quad K_4^*(t) = \frac{e_{22}^I K_4(t)}{\varepsilon_{22}^I K_0}, \quad (32)$$

with $K_0 = \sigma_0 \sqrt{\pi a}$ and a is the half length of an internal crack.

A fiber reinforced plate with a crack near the fiber

In the first example as shown in Fig. 1, we consider a fiber reinforced plate with a crack of length $2a$ near the fiber. The geometry of the cracked plate is determined by $h = 16.0mm$, $w = 20.0mm$, $r = 5.0mm$ and $a = r$.

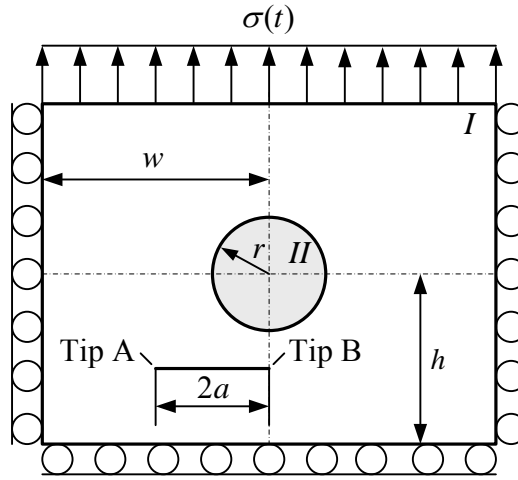


Figure 1: A fiber reinforced plate with a crack near the fiber

A tensile impact loading of the form $\sigma(t) = \sigma_0 H(t)$ is applied on the upper boundary, where $H(t)$ denotes the Heaviside step function. The normal components of the mechanical displacements are fixed on the left, right and lower boundary. As material for the matrix Epoxy is chosen, which has the following material parameters

$$\begin{aligned} C_{11} &= 8.0\text{GPa}, & C_{12} &= 4.4\text{GPa}, & C_{22} &= 8.0\text{GPa}, & C_{66} &= 1.8\text{GPa}, \\ \kappa_{11} &= 0.0372\text{C}/(\text{GVm}), & \kappa_{22} &= 0.0372\text{C}/(\text{GVm}) \end{aligned} \quad (33)$$

and the mass density $\rho = 1260\text{kg}/\text{m}^3$. For the fiber three different configurations are investigated. In the first case we consider a circular hole. In contrast, a piezoelectric Zirconate Titanate (PZT-5H) with the material constants

$$\begin{aligned} C_{11} &= 126.0\text{GPa}, & C_{12} &= 84.1\text{GPa}, & C_{22} &= 117.0\text{GPa}, & C_{66} &= 23.0\text{GPa}, \\ e_{21} &= -6.5\text{C}/\text{m}^2, & e_{22} &= 23.3\text{C}/\text{m}^2, & e_{16} &= 17.0\text{C}/\text{m}^2, \\ \kappa_{11} &= 15.04\text{C}/(\text{GVm}), & \kappa_{22} &= 13.0\text{C}/(\text{GVm}) \end{aligned} \quad (34)$$

and the mass density $\rho = 7500\text{kg}/\text{m}^3$ is applied in the second case for the fiber. To point out the influence of the hole and the piezoelectric fiber on the dynamic intensity factors Epoxy is chosen for the fiber in the third computation. This corresponds to a crack in a homogeneous

plate. The spatial discretization of the external boundary is performed by an element-length of $1.0mm$. The circular interface and the upper crack-face are approximated by 20 elements. A normalized time-step of $c_L\Delta t/h = 0.06$ is chosen, where c_L is the longitudinal wave velocity. The numerical results of the time-domain BEM are shown in Fig. 2.

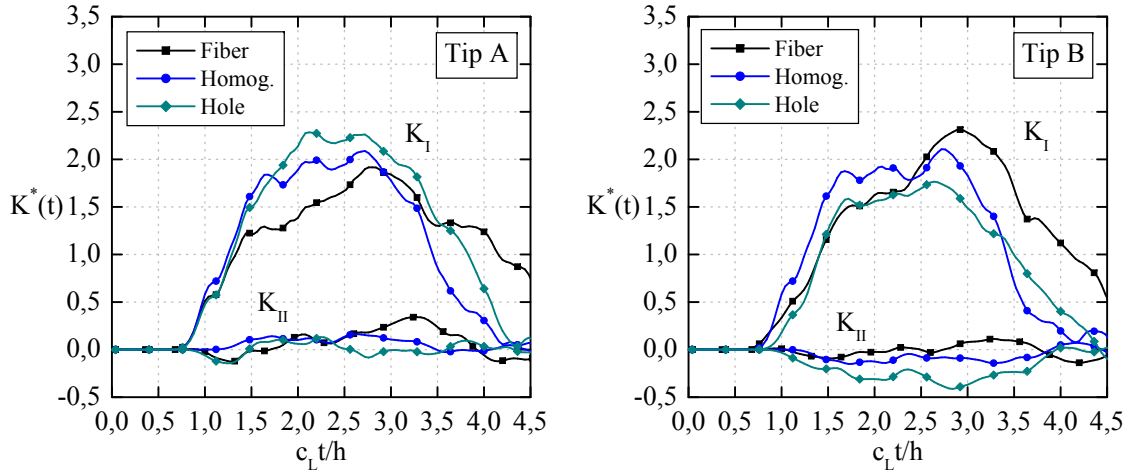


Figure 2: Normalized dynamic stress intensity factors of the three investigated configurations

The normalized dynamic mode-I and mode-II stress intensity factors of both crack-tips show a similar behavior. The curves of the homogeneous case are between the corresponding results of the fiber and hole configuration. The peak values of the left and the right crack-tip are nearly identical. In contrast, the mode-I stress intensity factors of the plate with the fiber and the hole show significant differences between both crack-tips. The right crack-tip is shielded by the hole which results in the lowest maximum peak value of all normalized dynamic mode-I stress intensity factor curves. On the other side the highest dynamic mode-II stress intensity factor is obtained. As clearly seen in Eqs. (33) and (34) the piezoelectric Zirconate Titanate has significant higher elastic constants than Epoxy. As a consequence the fiber increases the stiffness of the whole rectangular plate. Nevertheless the highest normalized dynamic mode-I stress intensity factor is obtained at the right crack-tip for the fiber configuration.

A square plate with a crack across the interface between the fiber and the matrix

In the next example a square plate with a crack across the interface between the fiber and the matrix is investigated. As depicted in Fig. 3 the cracked plate is subjected to an impact tensile loading $\sigma(t) = \sigma_0 H(t)$ normal to the crack-faces on the upper and the lower boundary. On the left and the right boundary the mechanical stresses are zero. The geometrical data are $h = 20.0mm$, $r = h/2$ and $2a = 4.8mm$.

As in the first example the material properties given in Eqs. (33) and (34) are considered for the matrix and the piezoelectric fiber. For spatial discretization the external boundary and the interface are discretized by a uniform mesh with an element-length about $1.0mm$. The upper crack-face is divided into 16 elements. A normalized time-step $c_L\Delta t/h = 0.06$ is used. The crack-faces are treated as electrically impermeable described by Eq. (12). The normalized dynamic intensity factors obtained by the time-domain BEM are given in Fig. 4.

As clearly observed the normalized dynamic stress intensity factors for the left and the right crack-tip show a quite different behavior. The dynamic stress intensity factor for the right crack-tip is considerably larger than that for the left crack-tip. This is very interesting since the

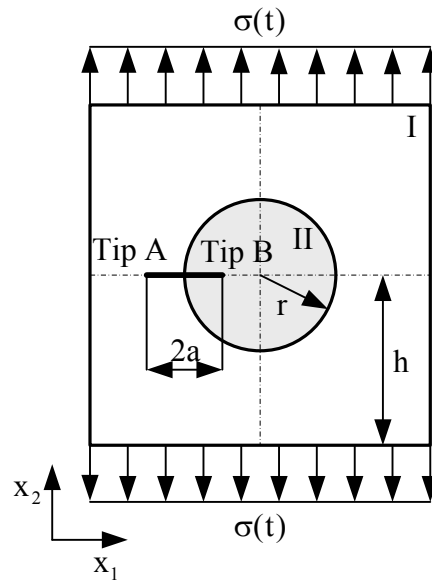


Figure 3: A crack across the interface between the fiber and the matrix in a square plate

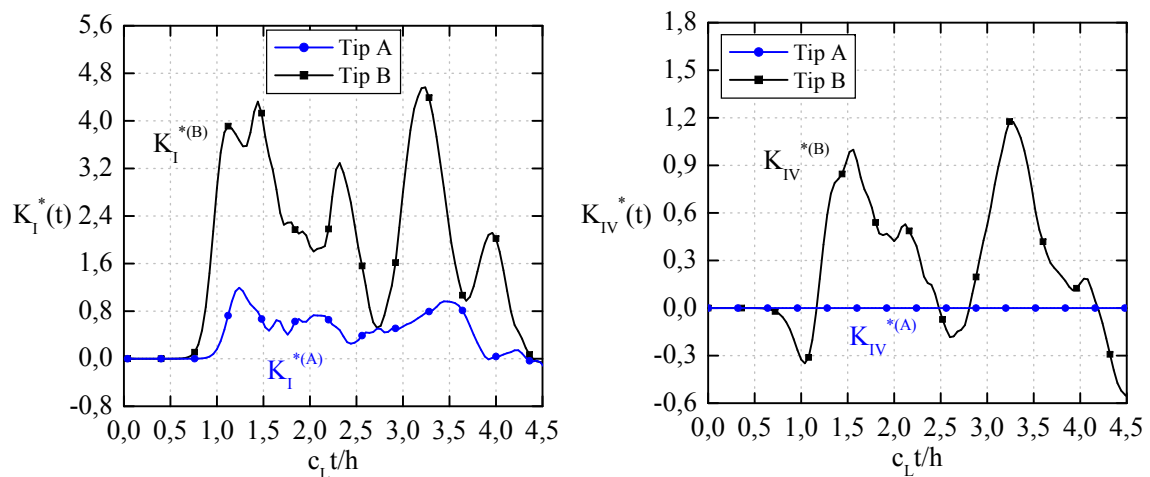


Figure 4: Normalized dynamic intensity factors of the left (A) and the right (B) crack-tip

elastic constants of the piezoelectric fiber (PZT-5H) are much higher than those of the matrix (Epoxy). The left crack-tip is inside the passive non-piezoelectric matrix and as a consequence the electrical displacement intensity factor is zero. Although the cracked plate is subjected to a pure mechanical impact loading a significant electrical displacement intensity factor is obtained at the right crack-tip. This is mainly induced by the coupling between the mechanical and the electrical field as well as the transient dynamic effects.

Interface crack in a square plate between the fiber and the matrix

In the last numerical example, we consider an interface crack in a square plate between the central fiber and the matrix as shown in Fig. 5. The geometry is prescribed by $h = 20.0mm$, $r = h/2$ and $2a = 14.0mm$. On the upper and the lower boundary an impact tensile loading $\sigma(t) = \sigma_0 H(t)$ is applied.

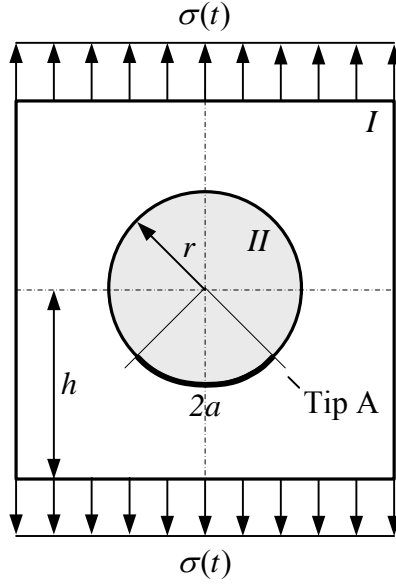


Figure 5: An interface crack in a square plate between the central fiber and the matrix

PZT-5H with the material properties given in Eq. (34) is used for the fiber (domain II). Barium Titanate (BaTiO_3) with the material constants

$$\begin{aligned}
 C_{11} &= 150.0\text{GPa}, & C_{12} &= 66.0\text{GPa}, & C_{22} &= 146.0\text{GPa}, & C_{66} &= 44.0\text{GPa}, \\
 e_{21} &= -4.35\text{C/m}^2, & e_{22} &= 17.5\text{C/m}^2, & e_{16} &= 11.4\text{C/m}^2, \\
 \kappa_{11} &= 9.87\text{C/(GVm)}, & \kappa_{22} &= 11.2\text{C/(GVm)}
 \end{aligned} \tag{35}$$

and the mass density $\rho = 5800\text{kg/m}^3$ is chosen for the matrix (domain I). The external boundary and the interface are divided into elements with a length about 1.0mm . The interface crack is divided into 20 elements. A normalized time-step $c_L\Delta t/h = 0.06$ is used.

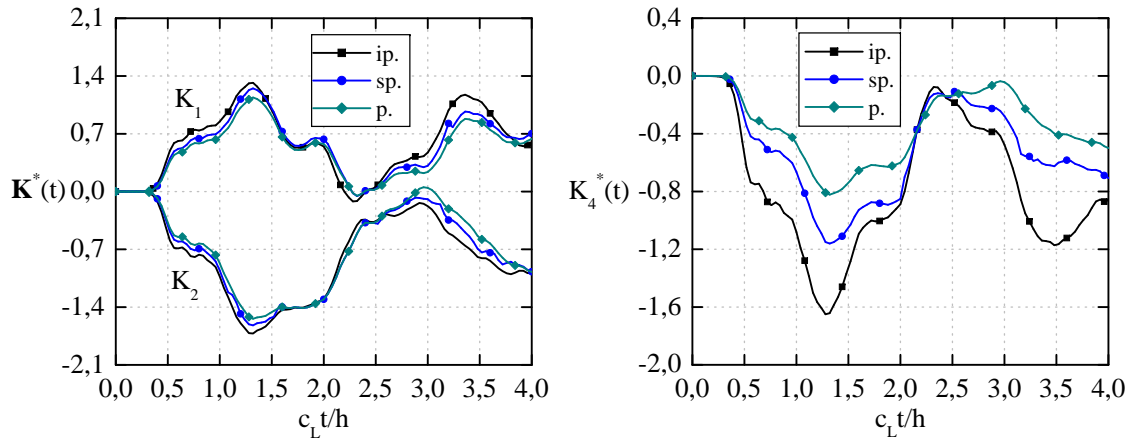


Figure 6: Normalized dynamic intensity factors of the interface crack

The normalized dynamic intensity factors for the impermeable (ip.), permeable (p.) and semi-permeable (sp.) crack-face boundary conditions (12)-(14) are shown in Fig. 6. The relative permittivity $\kappa_r = 40$ is used in the computations for the semi-permeable crack-face conditions. The elastic waves induced by the mechanical impact need some time to reach and excite the

crack. The global behavior of the dynamic intensity factors is very similar. It can be clearly seen, that the electrical permittivity of the medium inside the crack has a significant influence. Here again a high electrical displacement intensity factor is obtained even for a pure mechanical impact loading.

Conclusions

The transient dynamic analysis of piezoelectric fiber composites with cracks of arbitrary shape is presented in this paper. The developed symmetric Galerkin time-domain BEM is an attractive tool to compute the dynamic intensity factors. The formulation is general without limitations on the crack geometry, loading configuration and poling directions. The investigated numerical examples indicate a significant influence of the piezoelectric fiber and the transient dynamic loading on the normalized intensity factors.

Acknowledgement

This work is supported by the Slovak Academy of Sciences Project (SASPRO) 0106/01/01. The financial support is gratefully acknowledged.

References

- [1] Gellmann R., Ricoeur A. (2012) Some new aspects of boundary conditions at cracks in piezoelectrics. *Archive of Applied Mechanics* **82**, 841-852.
- [2] Hao T.H., Shen Z.Y. (1994) A new electric boundary condition of electric fracture mechanics and its applications. *Engineering Fracture Mechanics* **47**, 793-802.
- [3] Landis C.M. (2004) Energetically consistent boundary conditions for electromechanical fracture. *International Journal of Solids and Structures* **41**, 6291-6315.
- [4] Pak Y.E. (1990) Crack extension force in a piezoelectric material. *Journal of Applied Mechanics* **57**, 647-653.
- [5] Parton V.Z. (1976) Fracture mechanics of piezoelectric materials. *Acta Astronautica* **3**, 671-683.
- [6] Suo Z., Kuo C-M., Barnett D.M., Willis J.R. (1992) Fracture mechanics for piezoelectric ceramics. *Journal of the Mechanics and Physics of Solids* **40**, 739-765.
- [7] Wang C.-Y., Zhang Ch. (2005) 3-D and 2-D dynamic Green's functions and time-domain BIEs for piezoelectric solids. *Engineering Analysis with Boundary Elements* **29**, 454-465.
- [8] Wünsche M., García-Sánchez F., Sáez A., Zhang Ch. (2010) A 2D time-domain collocation-Galerkin BEM for dynamic crack analysis in piezoelectric solids. *Engineering Analysis with Boundary Elements* **34**, 377-387.
- [9] Wünsche M., Zhang Ch., García-Sánchez F., Sáez A., Sladek J., Sladek V. (2011) Dynamic crack analysis in piezoelectric solids with non-linear electrical and mechanical boundary conditions by a time-domain BEM. *Computer Methods in Applied Mechanics and Engineering* **50**, 2848-2858.